

A GLOBALLY CONVERGENT THIRD-ORDER NEWTON METHOD VIA UNIFIED SEMIDEFINITE PROGRAMMING SUBPROBLEMS

YUBO CAI*, WENQI ZHU†, CORALIA CARTIS†, AND GIOELE ZARDINI*

Abstract. We propose the Adaptive Levenberg-Marquardt Third-Order Newton Method (ALM-TON) method for unconstrained nonconvex optimization, providing the first globally convergent realization of the unregularized third-order Newton method. Unlike the standard Adaptive Regularization framework with third-order models (AR3), which enforces global behavior through a quartic term, ALM-TON employs an adaptive Levenberg-Marquardt (quadratic) regularization. This choice preserves a cubic model at every iteration, so that every subproblem is a tractable semidefinite programming (SDP). In particular, the ALM-TON-Simple variant requires exactly one SDP solve per iteration, making the per-iteration cost uniform and predictable.

Algorithmically, ALM-TON follows a mixed-mode strategy: it attempts an unregularized third-order step whenever the cubic Taylor model admits a strict local minimizer with adequate curvature, and activates (or increases) quadratic regularization only when needed to ensure that the model is well posed and the step is globally reliable. We establish global convergence and prove an $\mathcal{O}(\epsilon^{-2})$ worst-case evaluation complexity for computing an ϵ -approximate first-order stationary point. Numerical experiments show that ALM-TON enlarges the basin of attraction relative to classical baselines (gradient descent and damped Newton), and can progress on landscapes where second-order methods typically stagnate. When compared with a state-of-the-art third-order implementation (AR3-interp [14]), ALM-TON converges more consistently and often in fewer iterations. We also characterize the practical scalability limits of the approach, highlighting the computational bottlenecks introduced by current SDP solvers as dimension grows.

Key words. third-order Newton method; unconstrained nonconvex optimization; global convergence; adaptive regularization.

MSC codes. 90C26, 49M15, 65K10

1. Introduction. We consider unconstrained nonconvex optimization problems of the form

$$(1.1) \quad \min_{x \in \mathbb{R}^n} f(x),$$

which arise in diverse application domains, including neural network training [7, 8, 10, 21, 23], digital filter design [5, Chapter 9.4], and volatility estimation [18, Chapter 6]. Throughout, we assume that $f : \mathbb{R}^n \rightarrow \mathbb{R}$ is p -times continuously differentiable (for some $p \geq 1$) and bounded below by a finite value f_{low} .

Algorithms for (1.1) are typically iterative, producing a sequence $\{x_k\}$ via updates based on local models of f . The accuracy and geometry captured by these models depend strongly on the order of derivative information used. First-order methods use only ∇f and are inexpensive per iteration, while Newton-type methods incorporate $\nabla^2 f$ and often achieve fast local convergence when the quadratic model is reliable. Higher-order methods, and in particular third-order methods, incorporate derivatives of order $p \geq 3$ to build richer Taylor models that can remain accurate over a larger neighborhood and better reflect nonconvex curvature [1, 13]. This paper focuses on third-order methods.

A central challenge in nonconvex optimization is to combine *local efficiency* with *global reliability*. For first- and second-order methods, this is commonly achieved

*Laboratory for Information & Decision Systems, Massachusetts Institute of Technology, Cambridge, MA (yubocai@mit.edu; gzardini@mit.edu).

†Mathematical Institute, University of Oxford, UK (wenqi.zhu@maths.ox.ac.uk; cartis@maths.ox.ac.uk).

through line-search or trust-region globalization [17, 19, 31], which enforce sufficient decrease in the objective even when the local model is inaccurate far from the current iterate. Extending these ideas to higher-order models is more delicate: higher-degree Taylor polynomials can be nonconvex and even unbounded below, and their minimization subproblems can become substantially harder to solve robustly.

A principled approach to this difficulty is *adaptive regularization with higher-order models*. The adaptive regularization framework of order p (AR p) [9, 11] augments the p th-order Taylor model with a $(p + 1)$ st-degree regularizer,

$$\frac{\sigma_k}{p+1} \|x - x_k\|^{p+1}, \quad \sigma_k > 0,$$

and updates σ_k dynamically to guarantee progress. Under standard assumptions, AR p methods admit worst-case evaluation complexity bounds for achieving approximate first- and second-order stationarity [13, Theorem 3.6]. However, these bounds do not reflect the computational cost of solving the regularized subproblem at each iteration. In many regimes, the practical efficiency of AR p methods is dictated not by the number of evaluations but by the difficulty (and variability) of the inner subproblem solver.

Motivated by this computational bottleneck, [28] proposed an *unregularized third-order Newton method* that updates x_{k+1} using a strict local minimizer of the *cubic* Taylor model. A key enabling observation is that strict local minimizers of multivariate cubic polynomials can be computed via a SDP formulation [2, Section 6]. This yields a unified subproblem representation that depends only on the cubic coefficients. Under strong assumptions (e.g., strong convexity and Lipschitz continuity of the third derivative), the method achieves a cubic local convergence rate for sufficiently good initialization [28, Theorem 3.2].

Despite its appeal, the unregularized approach is inherently local and may be ill-posed away from a minimizer: the cubic Taylor model may fail to admit any strict local minimizer, rendering the SDP infeasible. A standard safeguard is to add a Levenberg–Marquardt (LM) quadratic term with a sufficiently large coefficient, which guarantees existence of a strict local minimizer of the resulting cubic model [28, Proposition 5.1]. This resolves well-posedness, but does not by itself provide a globalization mechanism or a worst-case complexity guarantee for general nonconvex objectives.

In this work we introduce ALMTON, which embeds the unregularized third-order Newton step into an *adaptive* framework that achieves global convergence. The key design choice is to replace the standard quartic regularization used in AR3 with an *adaptive LM quadratic* regularization. Crucially, this preserves a cubic model at every iteration, so that both unregularized and regularized steps can be computed through the same SDP template. Algorithmically, ALMTON follows a mixed-mode strategy: it prioritizes unregularized third-order steps when the cubic model is well behaved, and increases quadratic regularization only when necessary to restore well-posedness and enforce global progress. In section 5, we show that this strategy can exploit third-order curvature to traverse challenging nonconvex geometry with fewer iterations than classical second-order baselines and competitive third-order implementations, provided the dimension remains moderate.

1.1. Contributions and Organization. The primary contribution of this paper is the proposal of ALMTON, which to our knowledge represents the first globally convergent realization of the unregularized third-order Newton method. By substituting the standard quartic regularization of AR3 with an adaptive quadratic (Levenberg–

Marquardt) term, we maintain the cubic structure of the subproblem, enabling a unified solution via SDP. To the best of our knowledge, this is the first global convergence rate analysis for a high-order (cubic) algorithm whose every subproblem is a tractable SDP in nonconvex smooth optimization. We provide a rigorous complexity analysis, establishing that ALMTON achieves a worst-case evaluation complexity of $\mathcal{O}(\epsilon^{-2})$ for finding ϵ -approximate first-order stationary points, matching the canonical bounds for second-order methods while exploiting higher-order information.

On the empirical front, we conduct a comprehensive benchmarking study that goes beyond simple performance profiles. We explicitly isolate the geometric mechanism of the method, demonstrating in Subsection 5.3 that the inclusion of third-order curvature allows the algorithm to trace the geodesic of curved valleys where standard Newton methods stagnate. Furthermore, we provide a candid assessment of the method's scalability boundaries. Our stress tests on high-dimensional Rosenbrock functions (Subsection 5.2) reveal that while the method excels in low-dimensional, structurally complex regimes, the computational cost of the SDP subproblem creates a prohibitive bottleneck as the dimension increases, identifying clear targets for future algorithmic refinement.

The remainder of this paper is organized as follows. Section 2 introduces the necessary notation and reviews the unregularized third-order Newton method. Section 3 details the ALMTON framework, including the specific logic for step acceptance and regularization updates. Section 4 presents the global convergence analysis and complexity bounds. Numerical results, including robustness checks and trajectory analyses, are discussed in Section 5, followed by concluding remarks in Section 6.

2. Preliminaries and Notation.

Norms and tensor notation. Throughout this paper, $\|\cdot\|$ denotes the standard Euclidean norm on \mathbb{R}^n . For a tensor $T \in \mathbb{R}^{n \times \dots \times n}$ of order j , we define its induced operator norm as

$$(2.1) \quad \|T\|_{[j]} := \max_{\|v_1\|=\dots=\|v_j\|=1} |T[v_1, \dots, v_j]|.$$

Let $f : \mathcal{D} \subseteq \mathbb{R}^n \rightarrow \mathbb{R}$ be a function satisfying $f \in \mathcal{C}^p(\mathcal{D})$. The p th-order derivative of f at x is a symmetric p th-order tensor denoted by $\nabla^p f(x)$, with entries defined by

$$(2.2) \quad [\nabla^p f(x)]_{i_1, \dots, i_p} = \frac{\partial^p f(x)}{\partial x_{i_1} \dots \partial x_{i_p}}.$$

The notation $\nabla^p f(x)[s]^p$ represents the tensor acting on the vector $s \in \mathbb{R}^n$ repeated p times, i.e., $\nabla^p f(x)[s]^p = \sum_{i_1, \dots, i_p} [\nabla^p f(x)]_{i_1, \dots, i_p} s_{i_1} \dots s_{i_p}$. Specifically, for $p = 1$ and $p = 2$, we recover the gradient vector $\nabla f(x)$ and the Hessian matrix $\nabla^2 f(x)$, respectively.

Taylor models. For $p \geq 1$, the p th-order Taylor expansion of f around an iterate x_k is:

$$(2.3) \quad \Phi_{f, x_k}^p(x) := f(x_k) + \sum_{j=1}^p \frac{1}{j!} \nabla^j f(x_k)[x - x_k]^j.$$

Restricting our attention to $p = 3$ and defining the step $s := x - x_k$, the cubic model can be written explicitly using tensor slices:

$$(2.4) \quad \Phi_{f, x_k}^3(x) = f(x_k) + \nabla f(x_k)^\top s + \frac{1}{2} s^\top \nabla^2 f(x_k) s + \frac{1}{6} \sum_{i=1}^n s_i \cdot s^\top (\nabla^3 f(x_k))_i s,$$

where $(\nabla^3 f(x_k))_i \in \mathbb{R}^{n \times n}$ denotes the i -th matrix slice of the third derivative tensor. Specifically, this slice corresponds to the Hessian of the i -th partial derivative: $(\nabla^3 f(x_k))_i = \nabla^2(\partial_i f)(x_k)$. This representation aligns with the general form of a multivariate cubic polynomial introduced in Equation (2.5), where the coefficients are identified as $c = f(x_k)$, $b = \nabla f(x_k)$, $Q = \nabla^2 f(x_k)$, and $H_i = (\nabla^3 f(x_k))_i$.

Cubic polynomials and subproblem formulation. Generalizing the specific Taylor model structure, we consider the minimization of a generic multivariate cubic polynomial $\psi : \mathbb{R}^n \rightarrow \mathbb{R}$. Consistent with the tensor slice notation introduced in Equation (2.4), ψ is parameterized by a set of symmetric matrices $\{H_i\}_{i=1}^n \subset \mathbb{S}^n$ (representing the third-order interaction), a symmetric matrix $Q \in \mathbb{S}^n$, a vector $b \in \mathbb{R}^n$, and a scalar $c \in \mathbb{R}$:

$$(2.5) \quad \psi(x) = \frac{1}{6} \sum_{i=1}^n x_i \cdot x^\top H_i x + \frac{1}{2} x^\top Q x + b^\top x + c.$$

The gradient and Hessian of ψ then satisfy:

$$(2.6) \quad \nabla \psi(x) = \frac{1}{2} \sum_{i=1}^n x_i H_i x + Qx + b,$$

$$(2.7) \quad \nabla^2 \psi(x) = \sum_{i=1}^n x_i H_i + Q, \quad \nabla^3 \psi(x) = \{H_i\}_{i=1}^n.$$

A multivariate cubic polynomial $\psi : \mathbb{R}^n \rightarrow \mathbb{R}$ has either no local minimizer, exactly one strict local minimizer, or infinitely many non-strict local minimizers. Moreover, \bar{x} is a strict local minimizer iff $\nabla \psi(\bar{x}) = 0$ and $\nabla^2 \psi(\bar{x}) \succ 0$ [2, Theorem 3.1, Corollary 3.4]. If a strict local minimizer exists, it can be found by solving the following SDP [2, Section 6.3.2]:

$$(2.8) \quad \begin{aligned} \inf_{X \in \mathbb{S}^{n \times n}, x \in \mathbb{R}^n, y \in \mathbb{R}} \quad & \frac{1}{2} \text{Tr}(QX) + b^\top x + \frac{1}{2}y \\ \text{s.t.} \quad & \frac{1}{2} \text{Tr}(H_i X) + e_i^\top Qx + b_i = 0, \quad i = 1, \dots, n, \\ & v = \sum_{i=1}^n \text{Tr}(H_i X) e_i + Qx, \\ & \begin{bmatrix} \sum_{i=1}^n x_i H_i + Q & v \\ v^\top & y \end{bmatrix} \succeq 0, \quad \begin{bmatrix} X & x \\ x^\top & 1 \end{bmatrix} \succeq 0, \end{aligned}$$

where Tr denotes the trace and $\{e_i\}$ are the standard basis vectors. This SDP is strictly feasible when ψ has a unique strict local minimizer [28, Theorem 3.3], and can be solved to arbitrary accuracy in polynomial time [30].

2.1. Higher-order Optimization Algorithms.

Unregularized third-order Newton and LM regularization. Let $\Phi_{f,x_k}^3(\cdot)$ denote the cubic Taylor model at x_k (cf. Equation (2.4)). The Unregularized Third-Order Newton method [28, Algorithm 1] generates iterates $\{x_k\}$ analogously to classical Newton's method: it terminates when $\|\nabla f(x_k)\| \leq \epsilon$, and otherwise computes a higher-order Newton step by taking x_{k+1} as a *strict local minimizer* of the cubic model,

$$x_{k+1} \in \arg \min_x \Phi_{f,x_k}^3(x) \quad (\text{strict local minimum}).$$

When such a minimizer exists, it can be found via the unified SDP formulation in Equation (2.8). Far from a minimizer of f , however, Φ_{f,x_k}^3 may admit no (strict) local minimizer.

As noted in the discussion on cubic polynomials (cf. Equation (2.5)), the unregularized model Φ_{f,x_k}^3 is not guaranteed to possess a strict local minimizer; it may have no local minimizers or infinitely many non-strict ones, rendering the update step ill-defined. A standard safeguard is to augment the model with a LevenbergMarquardt (LM) regularization term and minimize instead:

$$m_{f,x_k}(x; \sigma) := \Phi_{f,x_k}^3(x) + \sigma \|x - x_k\|^2.$$

For sufficiently large σ , $m_{f,x_k}(\cdot; \sigma)$ has a local minimizer [28, Prop. 5.1]. A computable *sufficient* threshold ensuring existence is

$$(2.9) \quad \begin{aligned} g &:= (|\partial_1 f(x_k)|, \dots, |\partial_n f(x_k)|)^\top, \quad h := (\|(\nabla^3 f(x_k))_1\|_2, \dots, \|(\nabla^3 f(x_k))_n\|_2)^\top, \\ \alpha_{LM}(x_k) &:= \sqrt{\frac{3}{2} (\|g\| \|h\| + g^\top h)} - \min\{0, \lambda_{\min}(\nabla^2 f(x_k))\}. \end{aligned}$$

Any $\sigma \geq \alpha_{LM}(x_k)$ guarantees $m_{f,x_k}(\cdot; \sigma)$ has a (strict)local minimizer. We use α_{LM} as a *backstop* in the analysis; it need not be tight nor computed in practice.

Remark 2.1 (Unified subproblem solve). In both the unregularized and LM-regularized cases, the model remains *cubic*. Hence, whenever a (strict) local minimizer exists, we can solve the subproblem with the same SDP template (2.8). This unification is a key practical advantage carried throughout the paper.

ARp models. The ARp framework augments $\Phi_{f,\bar{x}}^p$ with a $(p+1)$ th-degree term:

$$\tilde{m}_{f,\bar{x}}^p(x, \tilde{\sigma}) = f(\bar{x}) + \sum_{j=1}^p \frac{1}{j!} \nabla^j f(\bar{x}) [x - \bar{x}]^j + \frac{\tilde{\sigma}}{p+1} \|x - \bar{x}\|^{p+1}.$$

For sufficiently large $\tilde{\sigma}$, the model $\tilde{m}_{f,\bar{x}}^p$ is bounded below (and coercive), guaranteeing that its global minimizer exists. The regularization parameter is adapted by a ratio test to ensure sufficient descent [9, 11–14]. In the special case $p = 3$ (AR3), the added term is quartic.

Trade-offs motivating our approach. The ARp philosophy is to guarantee robustness by *regularizing the model*: add a $(p+1)$ th-degree term with a sufficiently large coefficient $\tilde{\sigma}$, obtain a coercive surrogate whose global minimizer is guaranteed to exist, then select steps via a ratio test. This works well conceptually, but in practice it creates two frictions that are central to our design choices.

First, for $p = 3$ (AR3), the quartic regularization ensures coercivity, yet the resulting subproblem may remain nonconvex for moderate $\tilde{\sigma}$, and there is no single “one-size-fits-all” solver that covers the spectrum of problems and accuracies practitioners need. Implementations often rely on problem-specific routines or black-box smooth minimizers with their own heuristics. For the standard ARC ($p = 2$) subproblem, efficient iterative methods, such as the factorization-based MCM algorithm [11, Algorithm 6.1], are often used to find the global minimizer. For the AR3 ($p = 3$) subproblem, common approaches within the “AR3-BGMS” [14] variant include specialized algorithms such as Gencan [14, Procedure 4.2], formulations based on sums-of-squares (SOS) programming [1, 24, 32–34], and the use of AR2-based [14, Procedure 3.2, 4.1] methods as local solvers. By contrast, with an LM term the model remains

cubic for all σ . Whenever a (strict) local minimizer exists, whether unregularized or with LM, we can invoke the *same* SDP template (2.8), with shared tolerances, warm starts, and a consistent stopping interface.

Second, large regularization can erode local fidelity. As $\tilde{\sigma}$ grows, the regularizer increasingly dominates the Taylor terms, making predicted decrease less representative of the true objectives behavior, especially far from a solution. Empirically this can manifest as conservative steps, more unsuccessful iterations, and weaker correlation in the ratio test. In the LM-regularized cubic setting we still globalize, but the models polynomial degree and structure are preserved, which (i) improves calibration between predicted and actual decrease, and (ii) keeps step computation costs more predictable.

The practical upshot is a *mixed-mode* strategy: prefer an unregularized third-order step when the cubic model admits a strict local minimizer and curvature is adequate; otherwise, increase σ to cross a computable backstop (e.g., α_{LM}) that ensures existence of a local minimizer. This retains the desirable fast local behavior when available, while providing a principled globalization mechanism without switching sub-problem classes across iterations. Our focus on LM-regularized cubics is therefore not a rejection of AR*p* theory, but a complementary design that prioritizes a unified sub-problem solver and more stable model objective fidelity.

2.2. Standing assumptions and basic bounds. To facilitate the analysis, we adopt the following standard assumptions.

Assumption 1 (Smoothness and lower boundedness). Let $p \geq 3$ be fixed. We consider functions $f : \mathbb{R}^n \rightarrow \mathbb{R}$ satisfying:

1. $f \in \mathcal{C}^p(\mathbb{R}^n)$, i.e., f is p -times *continuously* differentiable;
2. f is bounded below by f_{low} ;
3. the p th-order derivative is Lipschitz (in operator norm): there exists $L \geq 0$ such that, for all $x, y \in \mathbb{R}^n$,

$$(2.10) \quad \|\nabla^p f(x) - \nabla^p f(y)\|_{[p]} \leq (p-1)! L \|x - y\|.$$

Assumption 1 aligns with the standing conditions in high-order methods (e.g., AR*p*) and yields the usual Taylor remainder bounds [9, 11, 13, 16, 32].

Assumption 2 (Uniform bounds along the iterates [32]). Along the sequence $\{x_k\}$ produced by the algorithm, there exist finite constants $\{\Lambda_j\}_{j=1}^p$ such that

$$\|\nabla^j f(x_k)\|_{[j]} \leq \Lambda_j, \quad \forall k \geq 0, j = 1, \dots, p.$$

Remark 2.2. Assumption 2 is *not* a global requirement; it only constrains the derivatives *along the iterates*.

We now recall the Taylor remainder bounds that will be used repeatedly.

LEMMA 2.3 (Taylor model bounds). *Under Assumption 1, for all $x, x_k \in \mathbb{R}^n$,*

$$(2.11) \quad f(x) \leq \Phi_{f, x_k}^p(x) + \frac{L}{p} \|x - x_k\|^{p+1}, \quad \|\nabla f(x) - \nabla \Phi_{f, x_k}^p(x)\| \leq L \|x - x_k\|^p.$$

Proof. See [9, Eq. (2.6)(2.7)]. □

COROLLARY 2.4 (Specialization to $p = 3$). *With $p = 3$ in Lemma 2.3, for $s := x - x_k$,*

$$f(x) \leq \Phi_{f, x_k}^3(x) + \frac{L}{3} \|s\|^4, \quad \|\nabla f(x) - \nabla \Phi_{f, x_k}^3(x)\| \leq L \|s\|^3.$$

3. ALMTON. Building on Section 2, we now specialize to $p = 3$ and give a complete description of our method. The key design choice is to *prefer* unregularized third-order steps whenever the cubic Taylor model admits a strict local minimizer with adequate curvature, and to *fall back* to an LM-regularized cubic otherwise. This preserves fast local behavior while providing a principled globalization mechanism, all within a unified cubic subproblem (solved by the SDP in (2.8)).

Cubic model with LM regularization. For any iterate x_k and regularization $\sigma \geq 0$, we define the cubic model

$$(3.1) \quad m_{f,x_k}(x; \sigma) := \Phi_{f,x_k}^3(x) + \sigma \|x - x_k\|^2,$$

so that $m_{f,x_k}(x_k; \sigma) = f(x_k)$ and

$$\nabla m_{f,x_k}(x; \sigma) = \nabla \Phi_{f,x_k}^3(x) + 2\sigma(x - x_k).$$

When σ is sufficiently large, $m_{f,x_k}(\cdot; \sigma)$ admits a local minimizer (see Equation (2.9)); conversely, when $\sigma = 0$, the model may be unbounded below or lack a local minimizer. Our framework exploits this structure by prioritizing the unregularized case ($\sigma = 0$) to exploit favorable local geometry, and increasing σ only when necessitated by the models behavior.

The ALMTON Framework. We first present the general control flow in Algorithm 3.1. This meta-algorithm encapsulates the initialization, termination criteria, and the acceptance ratio test. Crucially, it delegates the specific mechanisms for computing the trial step s_k and updating the regularization parameter σ_{k+1} to a specific *strategy* (denoted by \mathcal{U}).

Instantiating the Strategy. Algorithm 3.1 serves as a template for two distinct strategies: a *Simple* version and a *Heuristic* version. Without loss of generality, we restrict our **convergence analysis** to the **Heuristic** strategy, as it presents the more challenging theoretical case; the analysis extends naturally to the Simple variant, establishing the same worst-case complexity for both. The practical performance of these strategies is contrasted in section 5.

Strategy 1: The Simple Variant. Algorithm 3.2 adopts a minimalist approach. Upon an unsuccessful iteration, it triggers an exponential increase in σ_k at the outer level, and the new value is used in the next model phase.

The Simple strategy makes at most one SDP solve per iteration and delegates regularization growth entirely to the outer loop.

Strategy 2: The Heuristic Variant. The Heuristic strategy is motivated by the high computational cost of solving the SDP subproblem. Instead of rigidly rejecting any step failing the curvature condition, it uses an inner correction loop that actively searches for a valid regularization parameter $\tilde{\sigma}_k$ guaranteeing that the model is well-posed *before* evaluating the objective function. The inclusion of the spectral correction term $\tilde{\sigma} + (c - \bar{\lambda})_+$ allows for a geometry-informed adjustment of the regularization.

Remark 3.1. For the Heuristic strategy (Algorithm 3.3), the inner loop always terminates with a trial point \bar{x} satisfying the curvature and model-value conditions. However, the monotone increase of $\tilde{\sigma}$ can lead to *over-regularization*, forcing steps that are smaller than what the local landscape would otherwise allow. As a result, despite its theoretical robustness, the Heuristic variant may converge more slowly than the Simple variant in certain regimes; see Section 5 for detailed numerical evidence.

Algorithm 3.1 Adaptive Levenberg–Marquardt Third-Order Newton Method (ALMTON): General Framework

- 1: **Step 0: Initialization.** Given f , x_0 , tolerance $\epsilon > 0$, and constants $c > 0$, $l \in (0, c/6]$ (e.g., $l = c/10$), $\eta \in (0, 1)$, $\gamma > 1$, set $\sigma_0 := 0$, compute $f(x_0)$, and set $k := 0$.
- 2: **Step 1: Termination.** If $\|\nabla f(x_k)\| \leq \epsilon$, terminate with $x_\epsilon := x_k$. Otherwise, compute $\nabla f(x_k)$, $\nabla^2 f(x_k)$, $\nabla^3 f(x_k)$, and the threshold $\alpha_{LM}(x_k)$ from (2.9).
- 3: **Step 2: Step Calculation (Model Phase).** Execute the chosen strategy (e.g., **Simple** in Algorithm 3.2 or **Heuristic** in Algorithm 3.3) to obtain the trial step s_k and phase regularization $\tilde{\sigma}_k$.
- 4: **Step 3: Acceptance of the trial point.** Evaluate $f(\bar{x})$ and define the ratio

$$(3.2) \quad \rho_k = \begin{cases} \frac{f(x_k) - f(\bar{x})}{l \|s_k\|^2}, & \text{if } \tilde{\sigma}_k = 0, \\ \frac{f(x_k) - f(\bar{x})}{f(x_k) - m_{f,x_k}(\bar{x}; \tilde{\sigma}_k)}, & \text{if } \tilde{\sigma}_k > 0. \end{cases}$$

If $\rho_k \geq \eta$ (a **successful** iteration), set $x_{k+1} := \bar{x}$; otherwise set $x_{k+1} := x_k$.

- 5: **Step 4: Regularization parameter update.**

$$\sigma_{k+1} = \begin{cases} 0 & \text{if } \rho_k \geq \eta \quad (\text{success}), \\ \mathcal{U}(\sigma_k, \tilde{\sigma}_k) & \text{if } \rho_k < \eta \quad (\text{failure}), \end{cases}$$

where $\mathcal{U}(\cdot)$ denotes the strategy-specific update rule defined in Algorithm 3.2 or Algorithm 3.3. Increment $k \leftarrow k + 1$ and go to Step 1.

Algorithm 3.2 Strategy: ALMTON-Simple

- 1: **Mechanism: Step Calculation.**
- 2: Set $\tilde{\sigma} \leftarrow \sigma_k$. Attempt to compute a local minimizer \bar{x} of $m_{f,x_k}(\cdot; \tilde{\sigma})$.
- 3: **if** minimizer \bar{x} exists **and** $\lambda_{\min}(\nabla^2 f(\bar{x}) + 2\tilde{\sigma}I_n) \geq c$ **then**
- 4: Set $s_k := \bar{x} - x_k$ and $\tilde{\sigma}_k := \tilde{\sigma}$.
- 5: **else**
- 6: Set $s_k := 0$ and $\tilde{\sigma}_k := \tilde{\sigma}$. {Implicitly forces $\rho_k = -\infty$ }
- 7: **end if**
- 8: **Mechanism: Parameter Update** $\mathcal{U}(\sigma_k, \tilde{\sigma}_k)$.

$$\mathcal{U}(\sigma_k, \tilde{\sigma}_k) = \begin{cases} \max\{1, \alpha_{LM}(x_k)\}, & \text{if } \sigma_k = 0, \\ \gamma\sigma_k, & \text{if } \sigma_k > 0. \end{cases}$$

Phase notation. For clarity, we write $\tilde{\sigma}_k$ for the value of the regularization at the end of the model phase (i.e., the value with which \bar{x} and s_k are computed).

First- and second-order conditions at the trial point. Since \bar{x} is a (strict) local minimizer of the phase model

$$m_{f,x_k}(x; \tilde{\sigma}_k) = \Phi_{f,x_k}^3(x) + \tilde{\sigma}_k \|x - x_k\|^2,$$

Algorithm 3.3 Strategy: ALMTON-Heuristic

- 1: **Mechanism: Step Calculation.**
- 2: Set $\tilde{\sigma} \leftarrow \sigma_k$.
- 3: **repeat**
- 4: Compute minimizer \bar{x} of $m_{f,x_k}(\cdot; \tilde{\sigma})$. Let $\bar{\lambda} := \lambda_{\min}(\nabla^2 f(\bar{x}) + 2\tilde{\sigma}I_n)$.
- 5: **if** \bar{x} exists **and** $\bar{\lambda} \geq c$ **and** $m_{f,x_k}(\bar{x}; \tilde{\sigma}) \leq f(x_k)$ **then**
- 6: **break** {Valid step found}
- 7: **end if**
- 8: Increase $\tilde{\sigma} \leftarrow \max\{\alpha_{LM}(x_k), \gamma \max\{1, \tilde{\sigma}\}, \tilde{\sigma} + (c - \bar{\lambda})_+\}$.
- 9: **until** valid step found
- 10: Set $s_k := \bar{x} - x_k$ and $\tilde{\sigma}_k := \tilde{\sigma}$.
- 11: **Mechanism: Parameter Update** $\mathcal{U}(\sigma_k, \tilde{\sigma}_k)$.

$$\mathcal{U}(\sigma_k, \tilde{\sigma}_k) = \max\{\alpha_{LM}(x_k), \gamma \max\{1, \tilde{\sigma}_k\}\}.$$

the first- and second-order necessary conditions at \bar{x} read

$$(3.3) \quad \nabla_x m_{f,x_k}(\bar{x}; \tilde{\sigma}_k) = \nabla f(x_k) + (\nabla^2 f(x_k) + 2\tilde{\sigma}_k I_n) s_k + \frac{1}{2} \sum_{i=1}^n (s_k)_i \nabla_i^3 f(x_k) s_k = 0,$$

$$(3.4) \quad \nabla_x^2 m_{f,x_k}(\bar{x}; \tilde{\sigma}_k) = (\nabla^2 f(x_k) + 2\tilde{\sigma}_k I_n) + \sum_{i=1}^n (s_k)_i \nabla_i^3 f(x_k) \succeq 0.$$

Here $s_k := \bar{x} - x_k$ and $\{\nabla_i^3 f(x_k)\}_{i=1}^n$ are the matrix slices of the third derivative at x_k (cf. Section 2).

Model-phase invariants and basic descent. We next formalize the invariants guaranteed by the model phase in the Heuristic strategy and derive a per-iteration descent lemma that will be used in the complexity analysis.

PROPOSITION 3.2 (Model-phase invariants). *Fix k and suppose Step 2 in Algorithm 3.1 uses the Heuristic strategy Algorithm 3.3, returning $(\bar{x}, \tilde{\sigma}_k)$ with $s_k := \bar{x} - x_k$. Then:*

- (i) $m_{f,x_k}(\cdot; \tilde{\sigma}_k)$ admits a strict local minimizer at \bar{x} ;
- (ii) $\bar{\lambda}_k := \lambda_{\min}(\nabla^2 f(\bar{x}) + 2\tilde{\sigma}_k I_n) \geq c$;
- (iii) $m_{f,x_k}(\bar{x}; \tilde{\sigma}_k) < m_{f,x_k}(x_k; \tilde{\sigma}_k) = f(x_k)$.

Proof. If $m_{f,x_k}(\cdot; \tilde{\sigma})$ has no local minimizer, the phase increases $\tilde{\sigma}$ to at least $\alpha_{LM}(x_k)$, after which existence is guaranteed by [28, Prop. 5.1]. A local minimizer \bar{x} is (re)computed by the SDP in (2.8); hence (i) holds at phase exit. If $\bar{\lambda}_k < c$, the phase increases $\tilde{\sigma}$ and recomputes a local minimizer until the tests pass. Therefore, (ii) hold upon exit. Property (iii) follows directly from (i) and (ii). As \bar{x} is a strict local minima of $m_{f,x_k}(\cdot; \tilde{\sigma})$ with $\tilde{\sigma} \geq 0$, we have the model difference

$$\begin{aligned} f(x_k) - m_{f,x_k}(x_k; \tilde{\sigma}) &= f(x_k) - m_{f,x_k}(x_k; \tilde{\sigma}) + s_k^\top \nabla_x m_{f,x_k}(\bar{x}; \tilde{\sigma}) \\ &= \frac{1}{3} \sum_{i=1}^n s_k^\top (s_k)_i \nabla_i^3 f(x_k) s_k + \frac{1}{2} s_k^\top (\nabla^2 f(x_k) + 2\tilde{\sigma} I_n) s_k. \end{aligned}$$

From the second-order optimality condition ((3.4)) at \bar{x} , we also have

$$(3.5) \quad \frac{1}{2} s_k^\top \nabla_x^2 m_{f,x_k}(\bar{x}, \tilde{\sigma}) s_k = \frac{1}{2} \sum_{i=1}^n s_k^\top (s_k)_i \nabla_i^3 f(x_k) s_k + \frac{1}{2} s_k^\top (\nabla^2 f(x_k) + 2\tilde{\sigma} I_n) s_k \geq 0$$

since $\nabla_x^2 m_{f,x_k}(\bar{x}, \tilde{\sigma})$ is positive semidefinite (PSD). Assume, for contradiction, that $f(x_k) - m_{f,x_k}(\bar{x}, \tilde{\sigma}) \leq 0$. Then subtracting this from (3.5), we obtain:

$$(3.5) - (f(x_k) - m_{f,x_k}(\bar{x}, \tilde{\sigma})) = \frac{1}{6} \sum_{i=1}^n s_k^\top (s_k)_i \nabla_i^3 f(x_k) s_k \geq 0.$$

On the other hand, (ii) ensures $\bar{\lambda}_k \geq c > 0$. Since the algorithm assumes a non-trivial step ($s_k \neq 0$), we also have $\|s_k\| > 0$, which implies:

$$s_k^\top (\nabla^2 f(x_k) + 2\tilde{\sigma} I_n) s_k \geq c \|s_k\|^2 > 0.$$

Thus, we have:

$$f(x_k) - m_{f,x_k}(\bar{x}, \tilde{\sigma}) > 0,$$

which contradicts our assumption. Thus, the assumption is false and $m_{f,x_k}(\bar{x}; \tilde{\sigma}_k) < f(x_k)$ (iii) must hold. \square

LEMMA 3.3 (Exact identity for the unregularized model decrease). *If $\tilde{\sigma}_k = 0$ and \bar{x} is a strict local minimizer of $m_{f,x_k}(\cdot; 0)$ with $s_k := \bar{x} - x_k$, letting $H_k := \nabla^2 f(x_k)$ and $H_{\bar{x}} := \nabla^2 f(\bar{x})$ we have*

$$(3.6) \quad m_{f,x_k}(x_k; 0) - m_{f,x_k}(\bar{x}; 0) = s_k^\top \left(\frac{1}{6} H_k + \frac{1}{3} H_{\bar{x}} \right) s_k.$$

In particular, if $\lambda_{\min}(H_{\bar{x}}) \geq c$,

$$(3.7) \quad m_{f,x_k}(x_k; 0) - m_{f,x_k}(\bar{x}; 0) \geq \frac{c}{3} \|s_k\|^2 + \frac{1}{6} s_k^\top H_k s_k.$$

Proof. Let $\phi(t) := m_{f,x_k}(\bar{x} + t(x_k - \bar{x}); 0)$ for $t \in [0, 1]$ and $s := x_k - \bar{x}$. Then $\phi(0) = m_{f,x_k}(\bar{x}; 0)$ and, since \bar{x} is a strict local minimizer, $\phi'(0) = 0$. Because $m_{f,x_k}(\cdot; 0)$ is cubic, its Hessian varies affinely along the segment:

$$\nabla^2 m_{f,x_k}(\bar{x} + ts; 0) = t H_k + (1-t) H_{\bar{x}}.$$

Hence $\phi''(t) = s^\top (t H_k + (1-t) H_{\bar{x}}) s$. Taylors theorem with integral remainder (using $\phi'(0) = 0$) gives

$$\phi(1) - \phi(0) = \int_0^1 (1-t) \phi''(t) dt = s^\top \left(\int_0^1 (1-t) (t H_k + (1-t) H_{\bar{x}}) dt \right) s,$$

and $\int_0^1 (1-t)t dt = \frac{1}{6}$, $\int_0^1 (1-t)^2 dt = \frac{1}{3}$ yield (3.6). The bound (3.7) follows from $\lambda_{\min}(H_{\bar{x}}) \geq c$. \square

COROLLARY 3.4 (A conservative curvature-calibrated lower bound). *If $\tilde{\sigma}_k = 0$, $\lambda_{\min}(\nabla^2 f(\bar{x})) \geq c$, and $\lambda_{\min}(\nabla^2 f(x_k)) \geq -\frac{c}{2}$, then*

$$m_{f,x_k}(x_k; 0) - m_{f,x_k}(\bar{x}; 0) \geq \frac{c}{6} \|s_k\|^2.$$

Consequently, any fixed $l \in (0, c/6]$ makes $l \|s_k\|^2$ a valid lower bound on the unregularized model decrease.

Proof. Combine (3.7) with $s_k^\top H_k s_k \geq \lambda_{\min}(H_k) \|s_k\|^2 \geq -\frac{c}{2} \|s_k\|^2$. \square

Acceptance ratio: justification and calibration. When $\tilde{\sigma}_k > 0$, the denominator $f(x_k) - m_{f,x_k}(\bar{x}; \tilde{\sigma}_k)$ in (3.2) is the standard trust-region/ARC predicted decrease. When $\tilde{\sigma}_k = 0$, Lemma 3.3 and Corollary 3.4 yield

$$m_{f,x_k}(x_k; 0) - m_{f,x_k}(\bar{x}; 0) \geq (c/6) \|s_k\|^2$$

under a mild spectral check at x_k . We therefore fix $l \in (0, c/6]$ (e.g., $l = c/10$), so that $\rho_k \approx 1$ corresponds to well-predicted decrease in either regime and $l\|s_k\|^2$ is a conservative under-estimator in the unregularized case.

LEMMA 3.5 (Descent per successful iteration). *Let k be such that $\rho_k \geq \eta$ and $x_{k+1} = \bar{x}$. Then:*

(a) *If $\tilde{\sigma}_k = 0$, then $f(x_{k+1}) \leq f(x_k) - \eta l \|s_k\|^2$.*

(b) *If $\tilde{\sigma}_k > 0$, then $f(x_{k+1}) \leq f(x_k) - \eta(f(x_k) - m_{f,x_k}(\bar{x}; \tilde{\sigma}_k))$.*

In particular, $\{f(x_k)\}$ is nonincreasing and strictly decreases on every successful iteration.

Proof. By the definition of ρ_k in (3.2) and $\rho_k \geq \eta$,

$$f(x_k) - f(x_{k+1}) = \begin{cases} \rho_k l \|s_k\|^2, & \tilde{\sigma}_k = 0, \\ \rho_k (f(x_k) - m_{f,x_k}(\bar{x}; \tilde{\sigma}_k)), & \tilde{\sigma}_k > 0, \end{cases}$$

which yields (a)(b) immediately. Monotonicity follows since the right-hand sides are nonnegative. \square

Remark 3.6 (What counts as “successful” and how feasibility is checked). An iteration is *successful* only if Step 3 is reached with a bona fide trial point \bar{x} (hence $s_k = \bar{x} - x_k \neq 0$ unless already converged) and the mixed ratio test (3.2) yields $\rho_k \geq \eta$. Existence of a strict local minimizer of $m_{f,x_k}(\cdot; \sigma)$ is checked by attempting the SDP in (2.8); failure to meet solver tolerances or KKT residuals is interpreted as “no acceptable local minimizer” for the current σ and triggers a regularization increase within the model phase (Step 2). No ratio ρ_k is formed until the invariants in Proposition 3.2 are satisfied (for the Heuristic strategy).

Remark 3.7 (On the roles of c , l , and α_{LM}). The curvature floor $c > 0$ is a theoretical device used to (i) simplify global arguments (e.g., uniform step-size and decrease bounds) and (ii) calibrate the unregularized predictor in (3.2). Two consistent choices for l are common:

- *Minimal assumption (default in practice):* pick a small fixed $l \in (0, c/6]$ (e.g., $l = c/10$). This keeps the two ratio definitions numerically comparable; the global theory uses only the acceptance rule $\rho_k \geq \eta$.
- *Conservative under-estimator:* if one enforces the mild check $\lambda_{\min}(\nabla^2 f(x_k)) \geq -c/2$, Corollary 3.4 guarantees $m_{f,x_k}(x_k; 0) - m_{f,x_k}(\bar{x}; 0) \geq (c/6)\|s_k\|^2$, so any $l \leq c/6$ makes $l\|s_k\|^2$ a valid lower bound on the unregularized model decrease.

The LM backstop $\alpha_{LM}(x_k)$ (see (2.9)) is used only inside the model phase to guarantee existence of a local minimizer when σ is increased.

Remark 3.8 (Resetting to unregularized after success). After any successful iteration ($\rho_k \geq \eta$), we set $\sigma_{k+1} = 0$ to re-test the unregularized cubic at the next iterate. This is how ALMTON recovers fast local behavior whenever the cubic admits a well-conditioned local minimizer; if the unregularized model becomes ill-posed, the model phase (Step 2) increases σ until the backstops in Proposition 3.2 are met, after which the mixed ratio test (3.2) is applied again.

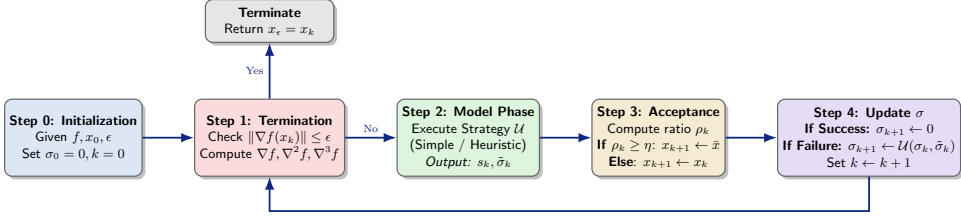


FIG. 1. **Flowchart of ALMTON.** The model phase (Step 2) escalates σ only as needed to enforce the invariants in Proposition 3.2. Step 3 applies the mixed ratio test (3.2). Step 4 resets σ after success, or increases it after failure, before the next iteration.

4. Convergence Rate of ALMTON. We organize the global convergence analysis of the ALMTON-Heuristic (Algorithm 3.1 with Algorithm 3.3) into four components. Our approach follows the standard paradigm for adaptive regularization methods [9, 12, 13, 15, 32].

Throughout this section, $\tilde{\sigma}_k$ denotes the *phase-closing* value from Step 2 (the value with which \bar{x} and s_k are obtained), while σ_{k+1} denotes the outer update in Step 4.

Part 1. Monotonicity of the algorithm: the sequence $\{f(x_k)\}$ is *monotone nonincreasing*. See Lemma 3.5 (Section 3) and Theorem 4.3 below (which also recalls Lemma 4.1 and Corollary 4.2).

Part 2. Uniform upper bound on the regularization: there exists $\tilde{\sigma}_{\max} < \infty$ such that $\tilde{\sigma}_k \leq \tilde{\sigma}_{\max}$ for all k (and hence $\sigma_k \leq \tilde{\sigma}_{\max}$ as well). See Lemma 4.5 and Lemma 4.6.

Part 3. Uniform lower bound on the step size on success: every successful iteration achieves a step of size at least a problem-dependent threshold, yielding a guaranteed decrease. See Lemma 4.7.

Part 4. A bound on unsuccessful iterations: the number of unsuccessful iterations is controlled by the number of successful ones, via a batching argument. See Lemma 4.8 and Theorem 4.9.

Combining monotonicity with the lower bound f_{low} and the bounds from Parts 2-4, Theorem 4.9 establishes global convergence and an evaluation complexity bound.

We start by making explicit the model bound enforced by the model phase.

LEMMA 4.1 (Model value bound returned by the model phase). *Under Assumption 1 and Algorithm 3.1, for every $k \geq 0$ the model phase (Step 2) returns $(\bar{x}, \tilde{\sigma}_k)$ with $s_k := \bar{x} - x_k$ such that*

$$(4.1) \quad m_{f,x_k}(\bar{x}; \tilde{\sigma}_k) = \Phi_{f,x_k}^3(\bar{x}) + \tilde{\sigma}_k \|s_k\|^2 \leq m_{f,x_k}(x_k; \tilde{\sigma}_k) = f(x_k).$$

Proof. This is exactly Proposition 3.2(iii), which is enforced by the model-phase loop in Step 2 before it returns $(\bar{x}, \tilde{\sigma}_k)$. \square

We next record the immediate consequence for the cubic Taylor gap.

COROLLARY 4.2. *For every $k \geq 0$,*

$$\Phi_{f,x_k}^3(x_k) - \Phi_{f,x_k}^3(\bar{x}) \geq \tilde{\sigma}_k \|s_k\|^2.$$

Proof. From (3.1), $m_{f,x_k}(x; \tilde{\sigma}_k) = \Phi_{f,x_k}^3(x) + \tilde{\sigma}_k \|x - x_k\|^2$. Evaluating at $x = x_k$ and $x = \bar{x}$ and subtracting, we get

$$m_{f,x_k}(x_k; \tilde{\sigma}_k) - m_{f,x_k}(\bar{x}; \tilde{\sigma}_k) = \Phi_{f,x_k}^3(x_k) - \Phi_{f,x_k}^3(\bar{x}) - \tilde{\sigma}_k \|s_k\|^2.$$

Use (4.1) to conclude the claim. \square

THEOREM 4.3 (Monotonicity of Algorithm 3.1). *Let Assumption 1 hold. Then, for all iterations $k \geq 0$, Algorithm 3.1 generates a sequence $\{x_k\}$ with:*

$$f(x_{k+1}) \leq f(x_k).$$

Moreover, if the iteration is successful ($\rho_k \geq \eta$), then with $s_k := \bar{x} - x_k$ and the phase-closing $\tilde{\sigma}_k$ we have:

$$\begin{cases} f(x_{k+1}) \leq f(x_k) - \eta l \|s_k\|^2, & \text{if } \tilde{\sigma}_k = 0, \\ f(x_{k+1}) \leq f(x_k) - \eta (f(x_k) - m_{f,x_k}(\bar{x}; \tilde{\sigma}_k)), & \text{if } \tilde{\sigma}_k > 0, \end{cases}$$

so the decrease is strict whenever the iteration is successful (and $s_k \neq 0$). If the iteration is unsuccessful ($\rho_k < \eta$), then $x_{k+1} = x_k$ and $f(x_{k+1}) = f(x_k)$. Consequently, $\{f(x_k)\}$ is monotone nonincreasing.

Proof. We distinguish two cases according to the acceptance test in Step 3.

Case 1 (successful iteration: $\rho_k \geq \eta$). In this case $x_{k+1} = \bar{x}$ and $s_k := \bar{x} - x_k$. Recall the mixed ratio (3.2) with the phase-closing regularization $\tilde{\sigma}_k$:

$$\rho_k = \begin{cases} \frac{f(x_k) - f(\bar{x})}{l \|s_k\|^2}, & \tilde{\sigma}_k = 0, \\ \frac{f(x_k) - f(\bar{x})}{f(x_k) - m_{f,x_k}(\bar{x}; \tilde{\sigma}_k)}, & \tilde{\sigma}_k > 0. \end{cases}$$

Since $\rho_k \geq \eta$ and $\eta \in (0, 1)$, we obtain in each subcase:

$$\tilde{\sigma}_k = 0: \quad f(x_k) - f(x_{k+1}) = \rho_k l \|s_k\|^2 \geq \eta l \|s_k\|^2.$$

$$\tilde{\sigma}_k > 0: \quad f(x_k) - f(x_{k+1}) = \rho_k (f(x_k) - m_{f,x_k}(\bar{x}; \tilde{\sigma}_k)) \geq \eta (f(x_k) - m_{f,x_k}(\bar{x}; \tilde{\sigma}_k)).$$

By Lemma 4.1 (the model value bound) we have $m_{f,x_k}(\bar{x}; \tilde{\sigma}_k) \leq f(x_k)$, so the term $f(x_k) - m_{f,x_k}(\bar{x}; \tilde{\sigma}_k)$ is nonnegative. Moreover,

$$f(x_k) - m_{f,x_k}(\bar{x}; \tilde{\sigma}_k) = (\Phi_{f,x_k}^3(x_k) - \Phi_{f,x_k}^3(\bar{x})) - \tilde{\sigma}_k \|s_k\|^2$$

because $m_{f,x_k}(x; \sigma) = \Phi_{f,x_k}^3(x) + \sigma \|x - x_k\|^2$ and $\Phi_{f,x_k}^3(x_k) = f(x_k)$. Applying Corollary 4.2 gives $\Phi_{f,x_k}^3(x_k) - \Phi_{f,x_k}^3(\bar{x}) \geq \tilde{\sigma}_k \|s_k\|^2$, hence $f(x_k) - m_{f,x_k}(\bar{x}; \tilde{\sigma}_k) \geq 0$. By construction of Step 2, Step 3 is only formed with a bona fide step $s_k \neq 0$ and positive denominator in the ratio, so the decrease is *strict* in both subcases:

$$\begin{cases} f(x_k) - f(x_{k+1}) \geq \eta l \|s_k\|^2 > 0, & \tilde{\sigma}_k = 0, \\ f(x_k) - f(x_{k+1}) \geq \eta (f(x_k) - m_{f,x_k}(\bar{x}; \tilde{\sigma}_k)) > 0, & \tilde{\sigma}_k > 0. \end{cases}$$

Case 2: Unsuccessful iteration ($\rho_k < \eta$). The iterate is rejected and $x_{k+1} = x_k$. Therefore $f(x_{k+1}) = f(x_k)$ and $x_{k+1} - x_k = 0$.

Combining the two cases, we conclude $f(x_{k+1}) \leq f(x_k)$ for all k , with strict inequality on every successful iteration. Hence $\{f(x_k)\}$ is monotone nonincreasing. \square

LEMMA 4.4. *Under Assumption 1 and Assumption 2, the threshold parameter α_k^{LM} defined in (2.9) satisfies*

$$(4.2) \quad \alpha_k^{LM} \leq \alpha_{\max} \stackrel{\text{def}}{=} \sqrt{3 \Lambda_1 \sqrt{n} \Lambda_3} + \Lambda_2.$$

Proof. The Euclidean norm of g_k is:

$$\|g_k\| = \sqrt{\sum_{i=1}^n (\partial_i f(x_k))^2} = \|\nabla f(x_k)\|,$$

since $\nabla f(x_k) = [\partial_1 f(x_k), \dots, \partial_n f(x_k)]^T$. By Assumption 2:

$$\|\nabla f(x_k)\| = \|\nabla^1 f(x_k)\|_{[1]} \leq \Lambda_1$$

As $\nabla_i^3 f(x_k) = \nabla^3 f(x_k) e_i$, the contraction of $\nabla^3 f(x_k)$ with the i -th basis vector e_i , yielding a second-order tensor (matrix). Therefore, we have

$$\|\nabla_i^3 f(x_k)\|_{[3]} = \|\nabla^3 f(x_k) e_i\|_{[2]} = \max_{\|v\|=\|w\|=1} |\nabla^3 f(x_k)[v, w, e_i]| \leq \|\nabla^3 f(x_k)\|_{[3]} \|e_i\| \leq \Lambda_3,$$

$$\|h_k\| = \sqrt{\sum_{i=1}^n \left(\|\nabla_i^3 f(x_k)\|_{[3]}\right)^2} \leq \sqrt{\sum_{i=1}^n \Lambda_3^2} = \sqrt{n} \Lambda_3.$$

Since g_k and h_k are non-negative vectors and by the Cauchy-Schwarz inequality, we can obtain the following:

$$g_k^T h_k = \sum_{i=1}^n |\nabla_i f(x_k)| \|\nabla_i^3 f(x_k)\|_{[3]} \leq \|g_k\| \|h_k\| \leq 2\Lambda_1 \sqrt{n} \Lambda_3.$$

For the rest part, we have

$$\|\nabla^2 f(x_k)\|_{[2]} = \max_{\|v\|=1} |\nabla^2 f(x_k)[v, v]| \leq \Lambda_2.$$

Thus, the eigenvalues of $\nabla^2 f(x_k)$ lie in the interval $[-\Lambda_2, \Lambda_2]$, which implies $\lambda_k \geq -\Lambda_2$. Now, consider $\min\{0, \lambda_k\}$. If $\lambda_k \geq 0$, then $\min\{0, \lambda_k\} = 0$; otherwise, if $\lambda_k < 0$, then $\min\{0, \lambda_k\} = \lambda_k \geq -\Lambda_2$. In both cases, we have

$$\min\{0, \lambda_k\} \geq -\Lambda_2 \iff -\min\{0, \lambda_k\} \leq \Lambda_2.$$

This gives us an upper bound for the second term of α_k^{LM} . Combining all the results obtained previously, we have

$$\alpha_k^{LM} = \sqrt{\frac{3}{2} (\|g_k\| \|h_k\| + g_k^T h_k) - \min\{0, \lambda_k\}} \leq \sqrt{3\Lambda_1 \sqrt{n} \Lambda_3} + \Lambda_2.$$

This establishes the uniform upper bound α_{\max} . \square

The uniform upper bound of $\tilde{\sigma}_k$ prevents the algorithm from diverging due to overly aggressive regularization. Before deducing such a bound, we first show that the trial step is uniformly bounded.

LEMMA 4.5 (Uniform upper bound for $\|s_k\|$). *Let Assumption 1 and Assumption 2 hold. Then, for all iterations $k \geq 0$,*

$$(4.3) \quad \|s_k\| \leq 4\Lambda_1 c^{-1}.$$

Proof. It is straightforward to verify that the model m has no local minimum so that $s_k = 0$ in **Step 2**. For the remaining two cases, we maintain control over the

minimum eigenvalue through the condition $\bar{\lambda}_k = \lambda_{\min}(\nabla_x^2 f(\bar{x}) + 2\sigma_k I_n) > c$, which ensures that:

$$\begin{aligned}
 0 &\geq m_{f,x_k}(\bar{x}, \sigma_k) - m_{f,x_k}(x_k, \sigma_k) \\
 &= \frac{1}{6} \sum_{i=1}^n s_k^\top (s_k)_i \nabla_i^3 f(x_k) s_k + \frac{1}{2} s_k^\top (\nabla^2 f(x_k) + 2\sigma_k I_n) s_k + s_k^\top \nabla f(x_k) \\
 &= \frac{2}{3} s_k^\top \nabla f(x_k) + \frac{1}{6} s_k^\top (\nabla^2 f(x_k) + 2\sigma_k I_n) s_k \quad (\text{by } -s_k^\top (3.3)) \\
 &\geq -\frac{2}{3} \|\nabla f(x_k)\| \|s_k\| + \frac{1}{6} \lambda_{\min}(\nabla^2 f(x_k) + 2\sigma_k I_n) \|s_k\|^2 \quad (\text{Cauchy-Schwarz})
 \end{aligned}$$

The mechanism of Algorithm 3.1 guarantees that, for all $k \geq 0$, we have

$$\begin{aligned}
 \frac{1}{6} \lambda_{\min}(\nabla^2 f(x_k) + 2\sigma_k I_n) \|s_k\|^2 &\leq \frac{2}{3} \|\nabla f(x_k)\| \|s_k\| \\
 \Rightarrow \|s_k\| &\leq 4 \frac{\|\nabla f(x_k)\|}{\lambda_{\min}(\nabla^2 f(x_k) + 2\sigma_k I_n)} \Rightarrow \|s_k\| \leq 4\Lambda_1 c^{-1}
 \end{aligned}$$

which gives us the desired results. \square

Now, we can deduce a simple upper bound on the regularization parameter σ_k .

LEMMA 4.6 (Uniform Bound on Regularization Parameter). *Under Assumptions 1 and 2, the regularization parameter σ_k in Algorithm 3.1 satisfies the uniform upper bound:*

$$(4.4) \quad \tilde{\sigma}_k \leq \tilde{\sigma}_{\max} \stackrel{\text{def}}{=} \max \left[\alpha_{\max}, \frac{16L\Lambda_1^2 c^{-2}}{3(1-\eta)} \right]$$

for all iterations $k \geq 0$, where α_{\max} is defined in (4.2).

Proof. We establish the bound by demonstrating that when $\tilde{\sigma}_k$ exceeds a critical threshold, the iteration must be successful, which subsequently prevents further growth of $\tilde{\sigma}_k$.

In the case where $\tilde{\sigma}_k = 0$, the parameter $\tilde{\sigma}_k$ is trivially upper bounded. Therefore, we restrict our analysis to the scenario with $\tilde{\sigma}_k > 0$ in this Lemma. A successful iteration requires ($s_k := \bar{x} - x_k$, $\tilde{\sigma}_k := \tilde{\sigma}$ and $x_{k+1} := \bar{x}$):

$$(4.5) \quad |\rho_k - 1| \leq \frac{|f(x_{k+1}) - \Phi_{f,x_k}^3(x_{k+1})|}{|f(x_k) - \Phi_{f,x_k}^3(x_{k+1})|} \leq \frac{L \|s_k\|^2}{3\tilde{\sigma}_k} \leq 1 - \eta,$$

where the inequalities follow from Corollary 2.4 and Lemma 4.1. As $\tilde{\sigma}_k \geq \frac{16L\Lambda_1^2 c^{-2}}{3(1-\eta)} \geq \frac{L \|s_k\|^2}{3(1-\eta)}$, the second inequality holds in that $\rho_k \geq \eta$ and $\tilde{\sigma}_{k+1} \leq \tilde{\sigma}_k$. Combining both conditions, we conclude that when:

$$\tilde{\sigma}_k \geq \max \left[\alpha_{\max}, \frac{16L\Lambda_1^2 c^{-2}}{3(1-\eta)} \right]$$

the iteration must be successful, causing $\tilde{\sigma}_{k+1} \leq \tilde{\sigma}_k$. This establishes the uniform upper bound $\tilde{\sigma}_{\max}$. \square

We now proceed to the third part of our analysis, where we aim to establish a uniform lower bound on the step size $\|s_k\|$. This guarantee is crucial as it ensures a minimum achievable reduction in the objective function value for successful iterations. The relationship between these quantities will be explicitly demonstrated in the subsequent development.

LEMMA 4.7 (Uniform Lower Bound on Step Size). *Under Assumption 1 and 2, for any successful iteration $k \geq 0$, the step size is bounded from below by:*

$$(4.6) \quad \|s_k\| \geq \min \left\{ 1, \frac{\|\nabla f(x_k + s_k)\|}{2\tilde{\sigma}_{\max} + L} \right\},$$

where $\tilde{\sigma}_{\max}$ is defined in (4.4).

Proof. Let the k th iteration be successful. From Assumption 1, we have the Taylor expansion of $\nabla f(x_k + s_k)$ around x_k ,

$$(4.7) \quad \nabla f(x_k + s_k) = \nabla f(x_k) + \nabla^2 f(x_k) s_k + \frac{1}{2} \sum_{i=1}^n (s_k)_i \nabla_i^3 f(x_k) s_k + R$$

where $R = \nabla f(x_k + s_k) - \nabla \Phi_{f, x_k}^3(x_k + s_k)$ is the residue of the Taylor expansion for the gradient. Combine (2.11), (3.4), and (4.7) implies $\nabla f(x_k + s_k) = R - 2\tilde{\sigma}_k s_k$, by the triangular inequality, we can obtain,

$$(4.8) \quad \|\nabla f(x_k + s_k)\| \leq L \|s_k\|^3 + 2\tilde{\sigma}_{\max} \|s_k\|.$$

As $\|s_k\| \geq 1$, $\|s_k\|^3$ is the dominant part and we already have a lower bound for steplength in this case. As $\|s_k\| < 1$, we have

$$\begin{aligned} 2\tilde{\sigma}_k \|s_k\| &\geq \|\nabla f(x_k + s_k)\| - \|R\| \geq \|\nabla f(x_k + s_k)\| - L \|s_k\|^3, \\ \Rightarrow \|s_k\| \left(2\tilde{\sigma}_k + L \|s_k\|^2 \right) &\geq \|\nabla f(x_k + s_k)\|, \\ \Rightarrow \|s_k\| &\geq \frac{\|\nabla_x f(x_k + s_k)\|}{2\tilde{\sigma}_k + L \|s_k\|^2}, \\ \Rightarrow \|s_k\| &\geq \frac{\|\nabla f(x_k + s_k)\|}{2\tilde{\sigma}_{\max} + L}. \end{aligned}$$

Combine our previous bound, giving us the desired lower bound in (4.6). \square

We now proceed to the final part of our analysis. First, we establish a bound on the number of unsuccessful iterations in terms of the number of successful ones. Then, we consolidate all the preceding results to complete the global convergence analysis.

We define $\mathcal{S}_k \stackrel{\text{def}}{=} \{0 \leq j \leq k \mid \rho_j \geq \eta\}$ as the index set encompassing all successful iterations from 0 to k . Additionally, we introduce $\mathcal{U}_k^1 \stackrel{\text{def}}{=} \{0 \leq j \leq k \mid \rho_j < \eta \text{ and } \sigma_j = 0\}$ and $\mathcal{U}_k^2 \stackrel{\text{def}}{=} \{0 \leq j \leq k \mid \rho_j < \eta \text{ and } \sigma_j > 0\}$ as the index sets capturing all unsuccessful iterations from 0 to k , corresponding to the distinct cases in the regularization parameter update scheme.

LEMMA 4.8 (Iteration Complexity Bound). *Under Assumption 1 and 2, Algorithm 3.1+Algorithm 3.3¹ satisfies the iteration complexity bound:*

$$(4.9) \quad k + 1 \leq \left(2 + \left\lceil \frac{\log \tilde{\sigma}_{\max}}{\log \gamma} \right\rceil \right) |\mathcal{S}_k| + 1 + \left\lceil \frac{\log \tilde{\sigma}_{\max}}{\log \gamma} \right\rceil$$

¹The bound (4.9) applies to the general ALMTON framework regardless of the σ -update strategy $\mathcal{U}(\cdot)$; only the constants $\tilde{\sigma}_{\max}$ and $|\mathcal{S}_k|$ depend on the specific strategy employed.

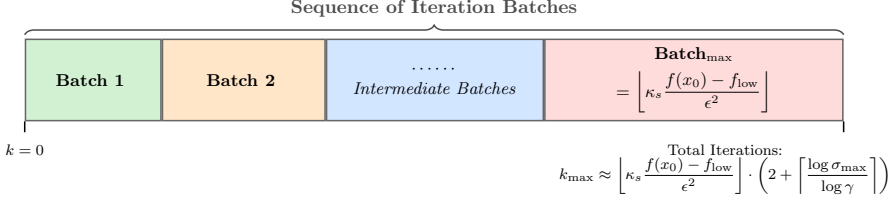


FIG. 2. Illustration of iteration batches in the optimization process.

where $|\mathcal{S}_k|$ and $|\mathcal{U}_k|$ denote the number of successful and unsuccessful iterations respectively.

Proof. We define a *batch* (example in Figure 2) as the sequence of iterations from an iteration i with $\tilde{\sigma}_i = 0$ to the next successful iteration j . Each batch consists of:

- (i) One successful iteration (the terminal iteration of the batch),
- (ii) At most one unsuccessful iteration with $\tilde{\sigma}_j = 0$ (belonging to \mathcal{U}_k^1),
- (iii) At most $\left\lceil \frac{\log \tilde{\sigma}_{\max}}{\log \gamma} \right\rceil$ unsuccessful iterations with $\tilde{\sigma}_j > 0$ (belonging to \mathcal{U}_k^2).

(iii) follows from the bound $\max \{ \alpha_{LM}(x_k), \gamma \max\{1, \tilde{\sigma}\}, \tilde{\sigma} + (c - \bar{\lambda}_k)_+ \} \geq \gamma$. This batch structure yields three key relationships:

$$(4.10) \quad k + 1 = |\mathcal{S}_k| + |\mathcal{U}_k^1| + |\mathcal{U}_k^2|$$

$$(4.11) \quad |\mathcal{U}_k^1| \leq |\mathcal{S}_k| + 1$$

$$(4.12) \quad |\mathcal{U}_k^2| \leq \left\lceil \frac{\log \tilde{\sigma}_{\max}}{\log \gamma} \right\rceil (|\mathcal{S}_k| + 1)$$

The inequality (4.11) follows because each batch contains at most one $\sigma = 0$ unsuccessful iteration, plus possibly one additional iteration at the beginning. The bound (4.12) arises because each σ_j grows geometrically by factor γ until reaching σ_{\max} .

Substituting (4.11) and (4.12) into (4.10) yields the desired complexity bound (4.9). \square

We now synthesize all previous analytical results to establish our main evaluation complexity theorem.

THEOREM 4.9. *Under Assumption 1 and 2, Algorithm 3.1 requires at most*

$$\left\lceil \kappa_s \frac{f(x_0) - f_{low}}{\epsilon^2} \right\rceil$$

successful iterations (each involving one evaluation of f and its 3 first derivatives) and at most

$$\left\lceil \kappa_s \frac{f(x_0) - f_{low}}{\epsilon^2} \right\rceil \left(2 + \left\lceil \frac{\log \tilde{\sigma}_{\max}}{\log \gamma} \right\rceil \right) + 1 + \left\lceil \frac{\log \tilde{\sigma}_{\max}}{\log \gamma} \right\rceil$$

iterations in total to produce an iterate $x_{\bar{\epsilon}}$ such that $\|\nabla_{x_{\bar{\epsilon}}}^1 f(x_{\bar{\epsilon}})\| \leq \epsilon$, where

$$\kappa_s \stackrel{\text{def}}{=} \frac{(2\tilde{\sigma}_{\max} + L)^2}{\eta l}.$$

Proof. For each successful iteration before termination, we have that

$$\begin{aligned} f(x_k) - f(x_k + s_k) &\geq \eta \left(\min\{l, 1\} \|s_k\|^2 \right) \geq \eta \min\{l, 1\} \min \left\{ 1, \frac{\|\nabla f(x_k + s_k)\|}{2\tilde{\sigma}_{\max} + L} \right\}^2 \\ &\geq \eta \min\{l, 1\} \min \left\{ 1, \frac{\epsilon^2}{(2\tilde{\sigma}_{\max} + L)^2} \right\} \end{aligned}$$

where the first inequality follows from (3.2) and Corollary 4.2, the second from Lemma 4.7, and the third from the stop condition. Normally, ϵ is far smaller than the scale of 1^{-6} and l is a small positive number, which implies $\min \left\{ 1, \frac{\epsilon^2}{(2\tilde{\sigma}_{\max} + L)^2} \right\} = \frac{\epsilon^2}{(2\tilde{\sigma}_{\max} + L)^2}$ and $\min\{l, 1\} = l$ by the assumption l is a small positive number. Thus we deduce that, for successful iterations and as long as termination does not occur,

$$f(x_0) - f(x_{k+1}) = \sum_{j \in \mathcal{S}_k} [f(x_j) - f(x_j + s_j)] \geq \frac{|\mathcal{S}_k|}{\kappa_s} \epsilon^2$$

from which the desired bound on the number of successful iterations follows. \square

Therefore, we proceed to demonstrate that under appropriate smoothness assumptions, Algorithm 3.1 is guaranteed to find an ϵ -approximate stationary point within at most $\mathcal{O}(\epsilon^{-2})$ iterations and function evaluations, as established by the complexity bound in Theorem 4.9.

5. Numerical Experiments. We now evaluate the numerical performance of the proposed ALMTON algorithm. All algorithms were implemented in Python 3.12.7, and experiments were conducted on a macOS machine with an Apple M2 Pro CPU (10 cores, 3.2 GHz) and 16 GB of RAM. For the SDP subproblems arising in ALMTON, we leverage MOSEK [6] as the primary solver, due to its state-of-the-art performance for interior-point methods. When MOSEK is unavailable, the implementation automatically falls back to SCS [26, 27] or CVXOPT [4].

To assess the efficiency of ALMTON, we compare it against a hierarchy of baselines ranging from first-order to state-of-the-art (SOTA) high-order methods:

- **First-order:** Gradient Descent (GD) with fixed stepsizes $\alpha \in \{0.01, 0.05\}$;
- **Second-order:** Damped Newton method, Newton-CG method;
- **Third-order/Regularized:** The unregularized third-order Newton method [28], and the adaptive regularization variants AR2-Interp and AR3-Interp [14].

Performance is reported in terms of both iteration counts and wall-clock time required to meet the stopping criterion. Unless otherwise noted, hyperparameters for the benchmark solvers (AR2-Interp and AR3-Interp) follow the default configurations in [14, Procedure 3.2], while ALMTON uses the default settings defined in Algorithm 3.1.

For termination, we enforce a tolerance of $\|\nabla f(x_k)\| \leq 10^{-8}$ for most test cases. The exception is Experiment 2, where the tolerance is relaxed to 10^{-6} to accommodate the ill-conditioning characteristic of high-dimensional landscapes. For all subproblem optimizations, we employ a dynamic solver precision (10^{-3} to 10^{-6}) to balance solution accuracy with computational cost. The evaluation of ALMTON, instantiated via its two proposed strategies, *Simple* and *Heuristic*, is structured as follows:

1. **Experiment 1** (subsection 5.1) investigates global stability and the basin of attraction on low-dimensional nonconvex landscapes, utilizing Dolan-Mor performance profiles for statistical analysis.
2. **Experiment 2** (subsection 5.2) tests scalability on Rosenbrock functions of varying dimensions.

3. **Experiment 3** (subsection 5.3) explores the algorithm’s ability to leverage third-order curvature on pathological geometries where second-order methods fail.

Preview of Results. In our tests, ALMTON exhibits strong robustness in low-dimensional regimes, making it particularly attractive for problems where each function evaluation is expensive (e.g., simulation-based models). However, we observe a practical computational boundary once the dimension exceeds roughly $n \approx 10$. This limitation does not arise from the outer iteration complexity, but from the rapidly increasing cost and numerical sensitivity of the SDP subproblems solved by off-the-shelf solvers (e.g., MOSEK, SCS) as n grows. As a result, while ALMTON is currently not competitive for high-dimensional problems, it proves highly stable and effective on small- to moderate-scale but structurally challenging nonconvex instances.

5.1. Experiment 1: Robustness and Basin of Attraction Analysis. The primary objective of this experiment is to empirically evaluate the size of the basin of attraction and the convergence efficiency of the proposed algorithms on classic nonconvex test functions. To achieve this, we employ a dense grid testing strategy to quantify convergence success rates and visualize the geometric shape of convergence basins. We utilize the test functions detailed in [28, Table 1].

For each test problem, we generate a uniform 30×30 grid of starting points x_0 spanning the rectangular domain $[X_{\min}, X_{\max}] \times [Y_{\min}, Y_{\max}]$ detailed in [28, Section 4.1]. This yields a total of $N = 900$ distinct initializations per function. An optimization run is classified as *successful* if the termination criterion $\|\nabla f(x_k)\| < 10^{-8}$ is satisfied within a budget of 100 iterations.

To provide a rigorous, aggregate assessment of the solvers beyond anecdotal case studies, we employ Dolan-Mor performance profiles [20]. This statistical tool allows us to evaluate the trade-off between efficiency and robustness across a large-scale test set. We construct a dense test set by treating every unique combination of a test function and a starting point as a distinct “problem instance”. With 4 test functions and a 30×30 grid of starting points per function, our test set P comprises a total of $|P| = 3600$ distinct optimization problems. This large sample size ensures that the resulting probability distributions are statistically significant. For a given solver s on problem $p \in P$, let $t_{p,s}$ denote the performance metric (e.g., number of iterations or problem solving time). If solver s fails to converge (termination criterion is not satisfied within maximum iterations) on problem p , we set $t_{p,s} = \infty$. The performance ratio is defined as:

$$(5.1) \quad r_{p,s} = \frac{t_{p,s}}{\min_{s'} t_{p,s'}},$$

which represents how much “worse” solver s performs compared to the best solver for that specific problem. The performance profile $\rho_s(\tau)$ is then the cumulative distribution function of these ratios:

$$(5.2) \quad \rho_s(\tau) = \frac{1}{|P|} |p \in P : r_{p,s} \leq \tau|.$$

In terms of interpretation, the intersection of the curve with the y -axis (at $\tau = 1$) captures the solver’s efficiency, representing the frequency with which it outperforms all competitors. A higher intercept thus denotes a greater likelihood of being the fastest solver. The profile’s right-tail behavior, particularly the asymptotic value as $\tau \rightarrow \infty$, corresponds to the robustness of each method. This limit indicates the total fraction of problems solved successfully, disregarding the magnitude of the performance

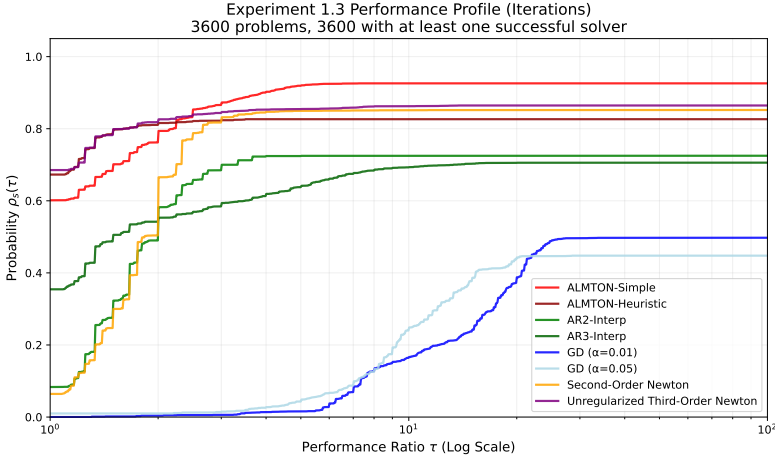


FIG. 3. *Dolan-Moré performance profiles based on iteration counts comparing ALMTON variants with baseline algorithms on a test set of $P = 3600$ problem instances. The curves represent the fraction of problems $\rho_s(\tau)$ solved by each algorithm within a factor τ of the best performance.*

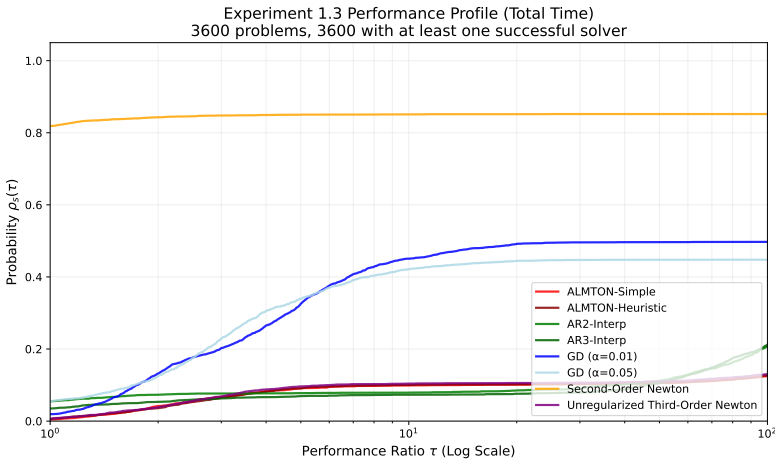


FIG. 4. *Dolan-Moré performance profiles based on total wall-clock time comparing ALMTON variants with baseline algorithms on a test set of $P = 3600$ problem instances. The curves represent the fraction of problems $\rho_s(\tau)$ solved by each algorithm within a factor τ of the best performance.*

ratio. The iteration complexity profile presented in Figure 3 provides empirical validation for the efficacy of incorporating third-order curvature. The ALMTON-Heuristic variant demonstrates immediate dominance with a high intercept at $\tau = 1$, solving approximately 70% of the test instances with the fewest iterations among all solvers. Notably, even the ALMTON-Simple variant, employing a straightforward update logic, achieves a win rate of approximately 60%, substantially outperforming the state-of-the-art AR3-Interp benchmark ($\approx 35\%$). As the performance ratio τ extends to 100, the ALMTON-Simple profile steadily climbs to a cumulative probability of 0.9, indicating successful convergence on the vast majority of the 3600 instances within the 100-iterations budget. In sharp contrast, the AR3-Interp curve saturates prematurely at a significantly lower reliability level (≈ 0.7). These findings collectively

underscore the superior stability and iteration efficiency of the ALMTON framework when navigating low-dimensional nonconvex landscapes.

Turning to the wall-clock time profile in Figure 4, we observe the intrinsic trade-off between iteration efficiency and per-step computational cost. As expected, the efficiency of ALMTON at $\tau = 1$ is lower than that of second-order methods, reflecting the overhead of solving an SDP subproblem compared to a linear system. This computational burden is not unique to our approach but is a characteristic shared by comparable high-order frameworks, such as AR3. Notably, as the performance ratio τ increases, the aggregate temporal performance of ALMTON converges toward that of the AR2-Interp and AR3-Interp benchmarks. Overall, while the Damped Newton method exhibits overwhelming dominance in raw computational speed, its reliability is notoriously compromised in nonconvex regimes. Specifically, second-order methods are prone to stagnation or divergence when encountering indefinite Hessians, saddle points, or narrow, winding valleysgeometric pathologies that we explicitly isolate and investigate in **Experiment 3**.

5.2. Experiment 2: High-Dimensional Rosenbrock Stress Test. While ALMTON demonstrates superior robustness in low-dimensional, geometrically complex landscapes, its performance characteristics shift dramatically as the problem dimension increases. To rigorously probe the scalability boundaries of the framework, we utilize the generalized Rosenbrock function:

$$(5.3) \quad f(x) = \sum_{i=1}^{n-1} [100(x_{i+1} - x_i^2)^2 + (1 - x_i)^2].$$

This function serves as an ideal stress test due to its ill-conditioned Hessian along the parabolic valley. We benchmark performance at $N = 5$ and $N = 20$ against L-BFGS (quasi-Newton) and Newton-CG (truncated Newton), employing both standard and randomly perturbed starting points.

Table 1 summarizes the comparative results.

TABLE 1

*Performance comparison on the Rosenbrock function across dimensions $N = 5$ and $N = 20$. Each solver is evaluated over 11 trials (1 standard initialization + 10 randomly perturbed seeds). “Success” denotes the convergence rate. Iters, Fevals, and Time are reported as medians over successful runs only. †Critical note for $N = 20$: The 9% success rate (1/11) corresponds to a single successful run from the standard initialization $x_0 = (-1, \dots, -1)^T$, which converged in only 2 iterations. All 10 randomly perturbed initializations failed due to `max_iterations_exceeded`. The reported metrics reflect this lone success and are **not** representative of typical performance.*

Solver	Dimension $N = 5$				Dimension $N = 20$			
	Success	Iters	Fevals	Time (s)	Success	Iters	Fevals	Time (s)
L-BFGS	100%	38	47	<0.01	100%	110	134	0.01
Newton-CG	100%	30	35	<0.01	100%	50	59	0.01
AR3-Interp	100%	21	294	0.20	100%	50	700	0.69
<i>ALMTON variants (SDP-based subproblem):</i>								
ALMTON	55%	795	3988	31.26	9%†	2†	10†	0.43†

Analysis of Scalability Bottlenecks. The data in Table 1 reveals a stark dichotomy. In the low-dimensional regime ($N = 5$), ALMTON remains operative but profoundly

inefficient. It achieves only a 55% success rate (6/11 trials) with a median of 795 iterations and 3988 function evaluations, which is $26\times$ more iterations than Newton-CG (30 iterations) and $113\times$ more function evaluations than L-BFGS (47 evaluations). The wall-clock time of 31.26 seconds dwarfs the sub-millisecond execution of classical methods by over four orders of magnitude.

The situation degenerates catastrophically at $N = 20$. The 9% “success rate” is statistically misleading. It reflects a *single* fortuitous convergence from the standard initialization $x_0 = (-1, \dots, -1)^\top$, which happens to lie near the curved valley floor. This lone success converged in merely 2 iterations, suggesting the SDP solver found a near-optimal step immediately. However, all 10 randomly perturbed starting points failed uniformly, exceeding the maximum iteration limit. In contrast, AR3-Interp (a non-SDP third-order method) and classical solvers maintain 100% reliability across all initializations.

We attribute this severe degradation not to the theoretical properties of the third-order model, but to the **numerical tractability of the SDP-based subproblem** in high-dimensional, ill-conditioned regimes. The root causes are threefold:

1. **SDP Solver Instability:** The Rosenbrock valley is characterized by extreme spectral disparity in the Hessian. As N increases, the condition number of the subproblem’s data matrices deteriorates. Current SDP solvers (e.g., MOSEK) struggle to resolve the strict complementarity and feasibility conditions required for a global cubic minimizer under such precision demands, leading to frequent solver failures or inaccuracies.
2. **Dimensionality Lifting and Algorithmic Complexity:** The reformulation of the n -dimensional cubic subproblem into the SDP (2.8) incurs a severe computational penalty. We provide a rigorous complexity analysis based on the specific structure of this SDP.

Problem dimensions. The SDP (2.8) involves: (i) decision variables $X \in \mathbb{S}^n$ ($\frac{n(n+1)}{2}$ entries), $x \in \mathbb{R}^n$, and $y \in \mathbb{R}$, yielding $N_{\text{var}} = \mathcal{O}(n^2)$ scalar variables; (ii) $m = 2n$ linear equality constraints (n stationarity conditions plus n auxiliary equations defining v); and (iii) two semidefinite constraints, each of size $(n+1) \times (n+1)$.

Theoretical lower bound (state-of-the-art IPM). According to the recent results by [22], the best-known theoretical complexity for solving an SDP with m linear constraints and a semidefinite block of size $n_{\text{sdp}} \times n_{\text{sdp}}$ is:

$$(5.4) \quad \mathcal{T}_{\text{IPM}}^{\text{theory}} = \tilde{\mathcal{O}}\left(\sqrt{n_{\text{sdp}}}\left(mn_{\text{sdp}}^2 + m^\omega + n_{\text{sdp}}^\omega\right)\log(1/\epsilon)\right),$$

where $\omega \approx 2.37$ is the matrix multiplication exponent. For our SDP with $m = 2n$ and $n_{\text{sdp}} = n + 1$, this yields:

$$(5.5) \quad \mathcal{T}_{\text{IPM}}^{\text{theory}} = \tilde{\mathcal{O}}\left(n^{3.5} + n^{0.5+\omega}\right)\log(1/\epsilon) = \tilde{\mathcal{O}}\left(n^{3.5}\right)\log(1/\epsilon),$$

since $0.5 + \omega \approx 2.87 < 3.5$. This represents a *theoretical lower bound* that is not yet achieved by practical solvers.

Practical complexity (MOSEK-style IPM). Commercial solvers such as MOSEK implement the standard primal-dual interior-point method, which forms and factorizes the *Schur complement* system at each iteration. The per-iteration cost is dominated by [3, 29]:

$$(5.6) \quad \mathcal{T}_{\text{iter}} = \mathcal{O}\left(m^2n_{\text{sdp}}^2 + m \cdot n_{\text{sdp}}^3\right).$$

Substituting $m = 2n$ and $n_{\text{sdp}} = n + 1$ gives $\mathcal{T}_{\text{iter}} = \mathcal{O}(n^4)$. The number of IPM iterations to reach ϵ -accuracy is $\mathcal{O}(\sqrt{n_{\text{sdp}}} \log(1/\epsilon))$ [25]. Hence, the **total practical complexity** is:

$$(5.7) \quad \mathcal{T}_{\text{SDP}}^{\text{practical}} = \mathcal{O}(n^{4.5} \log(1/\epsilon)).$$

Comparison with Newton-type methods. The truncated Newton method (Newton-CG) operates directly in \mathbb{R}^n , requiring only Hessian-vector products at cost $\mathcal{O}(n^2)$ per iteration. The polynomial gap between $\mathcal{O}(n^{4.5})$ and $\mathcal{O}(n^2)$ explains ALMTON’s computational bottleneck at $n = 20$.

3. **The Over-Regularization Trap:** To counteract the aforementioned ill-conditioning and maintain primal feasibility within the SDP, the adaptive logic in ALMTON (Step 2) is compelled to aggressively inflate the regularization parameter σ_k . A dominant σ_k effectively “washes out” the third-order curvature information, reducing the sophisticated cubic update s_k to a negligible magnitude. Consequently, the algorithm degenerates into an “over-damped” gradient descent, suffering from the dual penalty of slow convergence rates and exorbitant per-step computational costs.

These findings explicitly delineate the operational boundary of ALMTON. While it excels in navigating complex, low-dimensional non-convexities where standard methods fail, it is currently ill-suited for high-dimensional problems where the computational bottleneck shifts from function evaluation to subproblem resolution.

5.3. Experiment 3: Performance on High-Order Geometric Structures.

This experiment investigates the geometric mechanism behind the superior robustness of ALMTON. We specifically target scenarios where second-order methods fail due to the lack of sufficient curvature information.

5.3.1. Test Functions. We employ two specialized functions designed to “trap” second-order methods by incorporating significant third-order derivative features.

- **Slalom Function** [14, Example 1.1]: This function features a complex curvature structure that forces second-order algorithms into inefficient, zig-zagging paths along curved valley floors. In contrast, third-order methods are theoretically capable of identifying “shortcuts” through the landscape.
- **Hairpin Turn Function** [14, Appendix A.4]: Constructed to mimic a sharp hairpin turn, this function challenges optimization algorithms to anticipate rapid changes in direction. The mathematical definition involves a barrier function $b(x, x_{\min}, x_{\max})$ and a core structure $g(x, y)$ combined with a small slope $r = 3 \times 10^{-4}$ to ensure a unique minimizer.

$$b(x, x_{\min}, x_{\max}) = \begin{cases} (x - x_{\min})^4 & x \leq x_{\min} \\ 0 & x_{\min} < x < x_{\max} \\ (x - x_{\max})^4 & x \geq x_{\max} \end{cases}$$

The objective function is defined as:

$$(5.8) \quad f_{\text{hairpin}}(x, y) = g(x, y) + rx + 50b(x, -0.4, 0.5) + 50b(y, 0, 5)$$

where:

- $g(x, y) = h_2(x)h_4\left(x, \frac{2}{1+e^y}\right)$;
- $r = 3 \times 10^{-4}$ (a small slope term to prevent premature termination);
- $h_4(x, y)$ is a polynomial that interpolates to y for $x \in [-0.5, 0.5]$ and to 1 for $x \in \{-1, 1\}$.

Trajectory Analysis. Figure 5 visualizes the optimization paths originating from difficult starting points on the Slalom (Left) and Hairpin Turn (Right) functions, revealing fundamental differences in how algorithms navigate complex curvature.

On the **Slalom** function, second-order methods exhibit a characteristic pathology. Newton method (orange trajectory) becomes entrapped in severe oscillations, with frequent direction reversals as the local quadratic approximation fails to capture the changing curvature of the curved valley. AR2-Interp (blue trajectory) exhibits similar oscillatory patterns; while its adaptive regularization prevents outright divergence, the fundamental limitation of second-order curvature information remains. In sharp contrast, ALMTON (red trajectory) leverages the third-order derivative tensor $\nabla^3 f(x_k)$ to sense the “twist” in the valley floor. This higher-order information allows the cubic model to bend consistently with the landscape geometry, generating long, curvilinear steps that traverse the slalom with significantly higher *path efficiency*, defined as the ratio of straight-line displacement to total path length traveled.

A similar phenomenon manifests on the **Hairpin Turn**, where the barrier functions $b(x, x_{\min}, x_{\max})$ create a sharp bend that fundamentally challenges second-order methods. Newton and AR2 struggle to negotiate the turn, often stagnating with vanishingly small step sizes as the Hessian provides no anticipatory information about the impending direction change. In contrast, ALMTON anticipates the turn by sensing the asymmetry encoded in the third-order tensor, enabling smooth navigation of the hairpin with minimal oscillation and substantially higher overall efficiency.

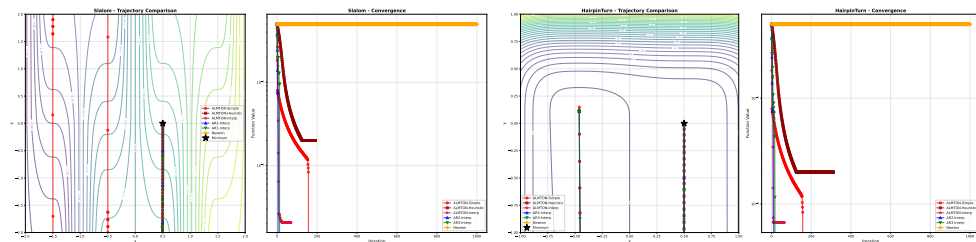


FIG. 5. *Trajectory comparison on high-order geometric structures. Left:* On the Slalom function, Newton method (orange) exhibits severe zig-zagging, while ALMTON (red) follows the valley’s geodesic with high path efficiency. *Right:* On the Hairpin Turn, ALMTON successfully navigates the sharp bend defined by the barrier functions, whereas second-order methods (Newton, AR2) stagnate or oscillate.

Statistical Failure of Second-Order Methods. To confirm that these observations are not artifacts of specific starting points, we conducted a dense grid search ($N = 400$ points) on the Hairpin Turn function. The results, summarized in Table 2, reveal a catastrophic failure of traditional methods.

These results expose a clear geometric hierarchy. The Second-Order Newton method succeeds only in 25.5% of cases, failing for 74.5% of the grid points due to iteration limits, which is consistent with its inability to “see around” the hairpin turn. The Unregularized Third-Order method improves success to 52% but remains unreliable because indefinite cubic models still appear frequently without global convergent framework. In contrast, interpolation-based AR2/AR3 achieve perfect reliability, indicating the importance of robust subproblem solvers. ALMTON-Simple also attains 100% success, but the large IQR reveals a bimodal behavior, where difficult starting points near the apex require substantially more effort, highlighting the computational price of SDP-based robustness. The heuristic variants (ALMTON-Heuristic and ALMTON-Interp) trade off stability for speed and fail in more than half of the

TABLE 2

Convergence statistics on the Hairpin Turn function ($N = 400$ grid points). Medians and IQRs are computed over successful runs. “Failure Reasons” lists dominant termination causes among unsuccessful runs. † The large IQR (465) indicates high variance: easy starts converge quickly, while starts near the hairpin apex require substantially more iterations.

Solver	Success	Iters [IQR]	Time (s) [IQR]	Failure Reasons
GD ($\alpha = 0.01$)	73.8% (295/400)	360 [205]	0.080 [0.046]	max_iter: 105
GD ($\alpha = 0.05$)	79.0% (316/400)	91 [68.3]	0.020 [0.023]	max_iter: 84
Second-Order Newton	25.5% (102/400)	9 [2]	0.002 [0.003]	max_iter: 298
Unreg. 3rd-Order Newton	52.0% (208/400)	14 [10]	0.625 [0.462]	max_iter: 152; sdp_fail: 40
AR2-Interp	100% (400/400)	9 [9]	0.055 [0.113]	–
AR3-Interp	100% (400/400)	10 [24.3]	0.099 [0.139]	–
ALMTON-Simple	100% (400/400)	20 [465]†	0.788 [9.373]	–
ALMTON-Heuristic	42.3% (169/400)	12 [5]	0.486 [0.305]	σ_{exc} : 203; max_iter: 28
ALMTON-Interp	49.8% (199/400)	6 [2]	0.319 [0.396]	σ_{exc} : 201

trials when the regularization threshold is exceeded.

6. Conclusion and Future Work. In this work, we have established ALMTON as a robust globalization framework that reconciles the fast local convergence of third-order methods with the rigorous stability required for general nonconvex optimization. Our empirical analysis confirms that by prioritising unregularized cubic steps, the algorithm not only secures a worst-case complexity of $\mathcal{O}(\epsilon^{-2})$ but also exhibits superior geometric intelligence. As evidenced by the trajectory analysis in Experiment 3, the incorporation of third-order tensor information enables ALMTON to successfully traverse complex, winding valleys, such as the “Hairpin Turn”, where traditional second-order methods suffer from structural stagnation.

However, our stress tests on high-dimensional Rosenbrock functions rigorously delineate the current operational boundary of the method. The computational burden of solving the cubic subproblem via exact semidefinite programming creates a distinct scalability barrier, typically limiting practical application to dimensions $n \leq 10$. This bottleneck is intrinsic to the dimensionality lifting required by the SDP reformulation (from \mathbb{R}^n to \mathbb{S}^{n+1}), which renders the per-iteration cost prohibitive for larger-scale problems despite the theoretical elegance of the solution.

Consequently, our future research agenda prioritizes dismantling this scalability bottleneck. We intend to investigate the replacement of the exact SDP solver with **approximate spectral solvers**, specifically leveraging **Krylov subspace methods** (such as the generalized Lanczos process) to solve the secular equation associated with the cubic model efficiently. Furthermore, to mitigate the memory and operation costs of forming the dense third-order derivative tensor, we plan to explore **tensor-train decompositions** and **randomized sketching techniques**. These extensions aim to preserve the geometric advantages of ALMTON while extending its applicability to high-dimensional optimization regimes.

Acknowledgments. We thank Dr. Yang Liu for helpful advice on the numerical experiments, and Dr. Runyu Zhang for valuable comments and revision suggestions.

References.

[1] A. A. AHMADI, A. CHAUDHRY, AND J. ZHANG, *Higher-order newton methods with polynomial work per iteration*, Advances in Mathematics, 452 (2024), p. 109808.

- [2] A. A. AHMADI AND J. ZHANG, *Complexity aspects of local minima and related notions*, Advances in Mathematics, 397 (2022), p. 108119.
- [3] F. ALIZADEH, J.-P. A. HAEBERLY, AND M. L. OVERTON, *Primal-dual interior-point methods for semidefinite programming: convergence rates, stability and numerical results*, SIAM Journal on Optimization, 8 (1998), pp. 746–768.
- [4] M. S. ANDERSEN, J. DAHL, AND L. VANDENBERGHE, *Cvxopt documentation*, tech. report, Release 1.2. 6. Tech. Rept, Tech. Rep, 2021.
- [5] A. ANTONIOU AND W.-S. LU, *Practical optimization: algorithms and engineering applications*, Springer, 2007.
- [6] M. APS, *The MOSEK Python Fusion API manual. Version 11.0.*, 2025, <https://docs.mosek.com/latest/pythonfusion/index.html>.
- [7] S. ARORA, N. COHEN, N. GOLOWICH, AND W. HU, *A convergence analysis of gradient descent for deep linear neural networks*, arXiv preprint arXiv:1810.02281, (2018).
- [8] A. S. BERAHAS, M. JAHANI, AND M. TAKÁČ, *Quasi-newton methods for deep learning: Forget the past, just sample*, arXiv preprint arXiv:1901.09997, 16 (2019).
- [9] E. G. BIRGIN, J. GARDENGI, J. M. MARTÍNEZ, S. A. SANTOS, AND P. L. TOINT, *Worst-case evaluation complexity for unconstrained nonlinear optimization using high-order regularized models*, Mathematical Programming, 163 (2017), pp. 359–368.
- [10] L. BOTTOU, F. E. CURTIS, AND J. NOCEDAL, *Optimization methods for large-scale machine learning*, SIAM review, 60 (2018), pp. 223–311.
- [11] C. CARTIS, N. I. GOULD, AND P. L. TOINT, *Adaptive cubic regularisation methods for unconstrained optimization. part i: motivation, convergence and numerical results*, Mathematical Programming, 127 (2011), pp. 245–295.
- [12] C. CARTIS, N. I. GOULD, AND P. L. TOINT, *Adaptive cubic regularisation methods for unconstrained optimization. part ii: worst-case function-and derivative-evaluation complexity*, Mathematical programming, 130 (2011), pp. 295–319.
- [13] C. CARTIS, N. I. GOULD, AND P. L. TOINT, *A concise second-order complexity analysis for unconstrained optimization using high-order regularized models*, Optimization Methods and Software, 35 (2020), pp. 243–256.
- [14] C. CARTIS, R. HAUSER, Y. LIU, K. WELZEL, AND W. ZHU, *Efficient implementation of third-order tensor methods with adaptive regularization for unconstrained optimization*, arXiv preprint arXiv:2501.00404, (2024).
- [15] C. CARTIS AND W. ZHU, *Cubic-quartic regularization models for solving polynomial subproblems in third-order tensor methods*, Mathematical Programming, (2025), pp. 1–53.
- [16] C. CARTIS AND W. ZHU, *Second-order methods for quartically-regularised cubic polynomials, with applications to high-order tensor methods: C. cartis, w. zhu*, Mathematical Programming, (2025), pp. 1–47.
- [17] A. R. CONN, N. I. GOULD, AND P. L. TOINT, *Trust region methods*, SIAM, 2000.
- [18] G. CORNUEJOLS, J. PEÑA, AND R. TÜTÜNCÜ, *Optimization methods in finance*, Cambridge University Press, 2018.
- [19] J. E. DENNIS JR AND R. B. SCHNABEL, *Numerical methods for unconstrained optimization and nonlinear equations*, SIAM, 1996.
- [20] E. D. DOLAN AND J. J. MORÉ, *Benchmarking optimization software with performance profiles*, Mathematical programming, 91 (2002), pp. 201–213.
- [21] I. GOODFELLOW, Y. BENGIO, AND A. COURVILLE, *Deep learning*, vol. 1, MIT

- press Cambridge, 2016.
- [22] H. JIANG, T. KATHURIA, Y. T. LEE, S. PADMANABHAN, AND Z. SONG, *A faster interior point method for semidefinite programming*, 2020, <https://arxiv.org/abs/2009.10217>, <https://arxiv.org/abs/2009.10217>.
 - [23] T. KURBIEL AND S. KHALEGHIAN, *Training of deep neural networks based on distance measures using rmsprop*, arXiv preprint arXiv:1708.01911, (2017).
 - [24] J. B. LASSERRE, *Global optimization with polynomials and the problem of moments*, SIAM Journal on optimization, 11 (2001), pp. 796–817.
 - [25] Y. NESTEROV AND A. NEMIROVSKII, *Interior-point polynomial algorithms in convex programming*, vol. 13, SIAM, 1994.
 - [26] B. O'DONOGHUE, *Operator splitting for a homogeneous embedding of the linear complementarity problem*, SIAM Journal on Optimization, 31 (2021), pp. 1999–2023.
 - [27] B. O'DONOGHUE, E. CHU, N. PARIKH, AND S. BOYD, *Conic optimization via operator splitting and homogeneous self-dual embedding*, Journal of Optimization Theory and Applications, 169 (2016), pp. 1042–1068, <http://stanford.edu/~boyd/papers/scs.html>.
 - [28] O. SILINA AND J. ZHANG, *An unregularized third order newton method*, arXiv preprint arXiv:2209.10051, (2022).
 - [29] M. J. TODD, *Semidefinite optimization*, Acta Numerica, 10 (2001), pp. 515–560.
 - [30] L. VANDENBERGHE AND S. BOYD, *Semidefinite programming*, SIAM review, 38 (1996), pp. 49–95.
 - [31] Y.-X. YUAN, *Recent advances in trust region algorithms*, Mathematical Programming, 151 (2015), pp. 249–281.
 - [32] W. ZHU AND C. CARTIS, *Global convergence of high-order regularization methods with sums-of-squares taylor models*, arXiv preprint arXiv:2404.03035, (2024).
 - [33] W. ZHU AND C. CARTIS, *Global optimality characterizations and algorithms for minimizing quartically-regularized third-order taylor polynomials*, 2025, <https://arxiv.org/abs/2504.20259>, <https://arxiv.org/abs/2504.20259>.
 - [34] W. ZHU AND C. CARTIS, *Sufficiently regularized nonnegative quartic polynomials are sum-of-squares*, 2026, <https://arxiv.org/abs/2601.20418>, <https://arxiv.org/abs/2601.20418>.